Available online at www.sciencedirect.com
ScienceDirect
Journal of the European Ceramic Society 29 (2009) 3249–3257
www.elsevier.com/locate/jeurceramsoc

Ho-doped $BaTiO_3$: Polymorphism, phase equilibria and dielectric properties of $BaTi_{1-x}Ho_xO_{3-x/2}$: $0 \leq x \leq 0.17$

Yang Liu, Anthony R. West *

Department of Engineering Materials, The University of Sheffield, Mappin Street, Sheffield S1 3JD, UK

Received 24 April 2009; accepted 25 May 2009
Available online 24 June 2009

Abstract

An extensive range of Ho-doped $BaTiO_3$ solid solution forms in which Ho substitutes for Ti with creation of oxygen vacancies. The effect of Ho substitution is to destabilise thermodynamically the high-temperature hexagonal polymorph of $BaTiO_3$. Nevertheless, at high Ho contents, the hexagonal polymorph forms as a kinetically stable intermediate before transforming to the thermodynamically stable cubic polymorph; its formation represents an example of Ostwald's rule of successive reactions. Samples fired at ~1400 °C and cooled in air are insulating and transform from ferroelectric to relaxor ferroelectric behaviour with increasing x.

Keywords: Barium titanate; Phase diagram; Permittivity; Electroceramics

1. Introduction

Electroceramic materials based on $BaTiO_3$ are among the most important in the electronics industry, with applications in multilayer ceramic capacitor, MLCC[1] and positive temperature coefficient of resistance, PTCR[2] devices. The properties of the ceramics depend on a number of factors associated with various dopant ions and the ceramic processing conditions. Very many doping studies have been reported; an overview of the key findings is given in the literature review in Ref. 3.

Donor dopants, defined as those that have higher charge than the ion that is being substituted, e.g. rare earth cations instead of Ba^{2+} or Nb^{5+} instead of Ti^{4+} can give rise to either semiconducting behaviour if the charge compensation is electronic and involves injection of electrons into the crystal structure, or insulating if the charge compensation mechanism is ionic and involves either generation of cation vacancies (primarily Ti vacancies) or the filling of pre-existing oxygen vacancies, associated with acceptor impurity cations. The conditions under which the two possible compensation mechanisms, electronic or ionic, occur is still a matter of controversy: the preferred mechanism appears to be electronic at low dopant content, switching to ionic at higher dopant content. However, complications arise since, depending on processing conditions, samples may lose oxygen at high temperatures, and, by the associated injection of electrons into the crystal structure, this provides an additional source of semiconductivity. As yet, it is not clear under which conditions the two mechanisms of electronic compensation, i.e. in response to direct donor doping or oxygen loss, occur.

Acceptor dopants, defined as those that have lower charge than the ion that is being substituted, e.g. Fe^{3+} instead of Ti^{4+}, generally achieve charge compensation through creation of oxygen vacancies and the resulting materials are electronically insulating. The exception is Ti^{3+}; since the single 3d electron associated with Ti^{3+} enters the 3d conduction band covering all Ti atoms of the $BaTiO_3$ lattice, the resulting acceptor-doped $BaTiO_3$, with ionic compensation by means of oxygen vacancies, is semiconducting.[4]

As well as the possible effect of dopants on the level of electronic conductivity, the permittivity and its temperature dependence are also dopant-sensitive. Most dopants reduce the Curie temperature, T_c, that is associated with the tetragonal–cubic, ferroelectric–paraelectric phase transition, and this is usually accompanied by a reduction in the permittivity maximum at T_c; La is an exception since, although T_c decreases, the permittivity at T_c increases with increasing La content.[5]

* Corresponding author. Tel: +44 114 222 5501; fax: +44 114 222 5943.
E-mail address: a.r.west@sheffield.ac.uk (A.R. West).

0955-2219/$ – see front matter © 2009 Elsevier Ltd. All rights reserved.
doi:10.1016/j.jeurceramsoc.2009.05.033

Processing conditions are critically important in controlling the electrical microstructure of undoped and doped $BaTiO_3$ ceramics; in particular, the oxygen loss that may occur at high temperatures and the partial or complete reoxidation on subsequent cooling leads to gradients in oxygen content, and therefore Ti^{3+} content, throughout the ceramics. Thus, it is in principle possible, by control of processing conditions, to obtain ceramics that are semiconducting throughout, insulating throughout or that have core–shell structures with insulating surfaces/grain boundaries and semiconducting grain cores.[6]

Given (a) the wide range of dopant ions that can enter the $BaTiO_3$ crystal lattice, with several possible charge compensation mechanisms, and (b) the importance of processing conditions, it is perhaps not surprising that the doping of $BaTiO_3$ continues to attract interest and controversy. Our objective is to obtain improved understanding of such materials by simultaneous, careful control of both doping mechanisms and processing conditions; this should then lead to the more effective optimisation of sample processing and fabrication and the ability to better tune the resulting properties.

This paper focuses on the effect of holmium as a dopant. Ho is one of the preferred rare earth dopants, since, depending on composition and processing conditions, room temperature resistivities as low as 3 Ω cm can be obtained. A detailed phase diagram study of the mechanism(s) of formation and extent of $BaTiO_3$ solid solutions doped with Ho, for samples fired under both oxidising and reducing conditions, has been reported.[7,8] One purpose of the present work is to better understand the correlation between electrical properties, solid solution mechanism and processing conditions; the phase diagram results[7,8] provide an excellent starting point for this study.

Ho^{3+} is an intermediate-sized cation capable of substituting on both octahedral Ti sites and 12-coordinate Ba sites. Since the charge on Ho^{3+} is different to that on both Ti^{4+} and Ba^{2+}, compensation mechanisms, or additional changes to the crystal/defect structure and stoichiometry, are required to preserve electroneutrality. These changes may be 'ionic', in which case the numbers of cations/oxygens are adjusted to achieve charge balance, or 'electronic' in which case electrons are either added to or removed from the crystal lattice to preserve electroneutrality. Here, we first discuss ionic compensation mechanisms and the associated changes to the defect structure and crystal stoichiometry.

The terms 'donor' and 'acceptor' doping are widely used in the ceramics literature, but there is ambiguity over the precise meaning of these terms. Some authors reserve the terms for situations in which charge compensation is electronic, as a consequence of which, there is usually a dramatic change in electrical conductivity. Others use the terms simply to imply that the substituting ion has either higher (donor) or lower (acceptor) charge than that of the ion being replaced, irrespective of whether charge compensation is ionic or electronic. To avoid ambiguity, we use the latter definition, although most of the discussion here refers to 'acceptor doping with ionic compensation' and 'donor doping with ionic compensation'. By using the latter definition, we avoid ambiguities associated with the Ti^{3+} dopant which is an acceptor (lower valence), with ionic compensation (oxygen vacancies), but which donates electrons to the Ti 3d conduction band, leading to semiconductivity.

The various doping mechanisms with ionic compensation that are possible in Ho-doped $BaTiO_3$ are summarised in Table 1, mechanisms 1–4; their compositional loci are represented on a ternary composition grid in Fig. 1, which is a section through the quaternary system Ba–Ti–Ho–O. Each substitution is, in principle, feasible, either as a single doping mechanism or in combination with another mechanism. We consider ions in their usual oxidation states, i.e. Ba^{2+}, Ti^{4+} and Ho^{3+}. All four ionic compensation mechanisms are associated with compositions on the ternary section $BaO–TiO_2–HoO_{3/2}$. The mechanisms are:

1. Acceptor doping of Ho onto Ti sites with ionic compensation through creation of oxygen vacancies.
2. Double substitution of Ho onto both Ba and Ti sites, in equal amounts. Each individual substitution is aliovalent since Ho has different charge to both Ba and Ti, but the net effect of the double substitution is isovalent since electroneutrality is retained and the overall stoichiometry remains at ABO_3.

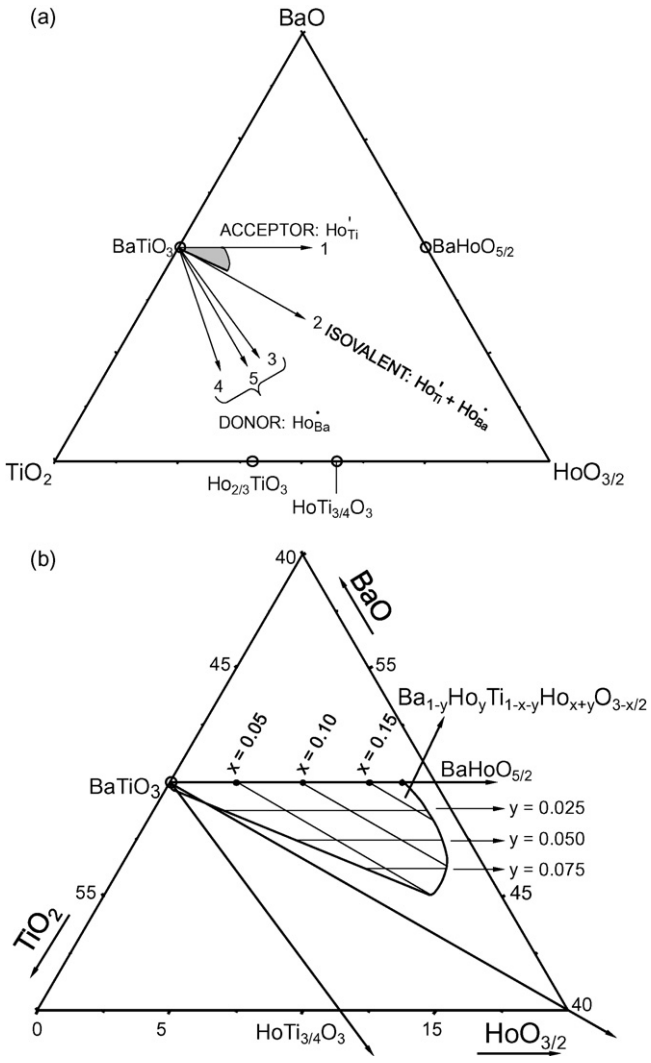

Fig. 1. Composition triangle $BaO–TiO_2–Ho_2O_3$ showing (a) possible doping mechanisms with the reported area of $BaTiO_3$ solid solutions shown shaded and (b) expanded solid solution area showing compositional grid superposed.

Table 1
Possible mechanisms for doping $BaTiO_3$ with Ho.

	Doping mechanism	Structural consequences	Formula	End-member (real or hypothetical)
1.	Acceptor, Ho'_{Ti}	Oxygen vacancies, $V_O^{\bullet\bullet}$	$BaTi_{1-x}Ho_xO_{3-x/2}$	$BaHoO_{2.5}$
2.	Stoichiometric double doping, $Ho^{\bullet}_{Ba} + Ho'_{Ti}$	Retain ABO_3 stoichiometry	$Ba_{1-y}Ti_{1-y}Ho_{2y}O_3$	Ho_2O_3
3,4.	Donor doping, $Ho^{\bullet}_{Ba}$	Cation vacancies (V'''_{Ti} or V''_{Ba})	$Ba_{1-z}Ho_zTi_{1-z/4}O_3$ or $Ba_{1-3\omega}Ho_{2\omega}TiO_3$	$HoTi_{3/4}O_3$ or $Ho_{2/3}TiO_3$
5	Donor doping, electronic compensation with Ti^{3+}	Retain ABO_3 stoichiometry	$Ba_{1-v}Ho_vTiO_3$	$HoTiO_3$

3,4. Donor doping of Ho onto Ba sites with ionic compensation, leading to either Ti vacancies (3) or Ba vacancies (4). In the case of impure $BaTiO_3$ that contains acceptor dopants and associated oxygen vacancies,[9] donor doping of Ho onto Ba sites may also involve compensation by excess oxygen ions which fill the pre-existing oxygen vacancies. This is not included in Fig. 1 or Table 1, since it is not a mechanism that is appropriate for pure, stoichiometric $BaTiO_3$.

Experimental studies on $BaTiO_3$ doped with Ho,[7] in air at 1400–1500 °C, have shown the existence of a solid solution area, shaded, Fig. 1(a) and on expanded scale in Fig. 1(b). A combination of two mechanisms is needed to describe a solid solution area. In this case, there is extensive solid solution with mechanism 1, but the solid solution is most extensive in the region between mechanisms 1 and 2. This indicates that Ho substitution for Ti is the preferred mechanism, but that substitution can be extended further through combination with the double substitution mechanism 2. There was little evidence of substitution by mechanisms 3 and 4 in air, for which Ho would substitute exclusively onto Ba sites; by contrast, significant substitution onto Ba sites was found in a reducing atmosphere,[8] probably with direct replacement of Ho^{3+} for Ba^{2+} and charge balance by reduction of Ti^{4+} to Ti^{3+}, mechanism 5, Fig. 1(a), Table 1.

In order to describe structurally the compositional extent of the solid solutions, we have superposed a compositional grid onto the solid solution area in Fig. 1(b) with two variables, x and y, in the general solid solution formula, $(Ba_{1-y}Ho_y)(Ti_{1-x-y}Ho_{x+y})O_{3-x/2}$. The limiting axes are the acceptor doping mechanism, 1, with x as a variable and the double substitution mechanism, 2, with y as a variable. Almost all compositions in the solid solution area can be represented in terms of positive values of x and y. For donor doping with either ionic compensation, 3 and 4, or with electronic compensation, 5, different general formulae are needed, Table 1.

From the phase diagram results,[7] the solid solution limit according to mechanism 1 is $x = 0.15$, $y = 0$; the most extensive solid solution, with a combination of mechanisms 1 and 2, occurs at $x = 0.05$, $y = 0.09$; with donor doping, mechanism 3, the solid solution limit was given as $z = 0.014$ at 1400 °C. For samples fired under reducing conditions at 1400 °C,[8] the solid solution extent with mechanism 1 was less, $x = 0.09$, was the same for a combination of mechanisms 1 and 2 and was greater for a donor doping mechanism; in the latter case, however, compensation was believed to be electronic, as indicated above, with the presumed formula $Ba_{1-v}Ho_vTiO_3$, number 5.

2. Experimental

Samples were synthesised by solid state reaction using $BaCO_3$ (Aldrich 99%), TiO_2 (Aldrich 99%) and Ho_2O_3 (Aldrich 99.9%), which were dried prior to weighing at 180, 800 and 800 °C, respectively. Samples totalling ca. 5 g were mixed with acetone manually in a mortar and pestle, dried and fired in Pt crucibles, initially overnight at 1050 °C to decarbonate the $BaCO_3$ and initiate reaction, followed by temperatures in the range 1350–1550 °C for several days in air with daily regrinding. For phase diagram studies on the cubic to hexagonal transition region, samples were heated isothermally for various periods of time and cooled rapidly to room temperature by withdrawing samples from the furnace and allowing them to cool in air.

Samples were characterised by X-ray powder diffraction, XRD, using a Stoe Stadi-P image plate detector (Stoe and Cie Gmbh, Darmstadt) for routine analysis and with a small linear position sensitive detector for accurate lattice parameter determination, Cu $K\alpha_1$ radiation, $\lambda = 1.5406$ Å. The tetragonal to cubic phase transition was monitored by differential scanning calorimetry (Polymer Laboratory DSC auto) between room temperature and 200 °C, heating rate 10 °C min^{-1}.

Pellets for electrical property measurements were pressed uniaxially in a stainless steel die, followed by cold isostatic pressing; for sintering, pellets were placed on Pt foil in different atmospheres and temperatures in the range 1350–1550 °C. Electrodes on opposite pellet faces were fabricated either from gold paste, which was dried and fired at 900 °C, or using In–Ga liquid alloy that was applied at room temperature and used directly. Fixed frequency measurements were made as a function of temperature using a Hewlett Packard HP4284A high precision LCR meter. Variable frequency impedance measurements over the range 10 Hz to 1 MHz, were made over the temperature range −263 to 500 °C under different atmospheric conditions using an HP impedance analyser.

3. Results and discussion

3.1. Phase diagram study of Ho-doped $BaTiO_3$ with composition $BaTi_{1-x}Ho_xO_{3-x/2}$

Using the phase diagram results reported in Ref. 7, based on heating samples at 1400–1500 °C in air, as a starting point, preliminary experiments were carried out to establish the conditions necessary to achieve complete reaction and therefore, equilib-

rium products. Synthesis of pure $BaTiO_3$ typically required temperatures of 1300–1400 °C in air for 24–48 h to achieve high-quality phase-pure samples. On addition of Ho as an acceptor dopant, with ionic compensation and solid solution formula according to mechanism 1, it was found that increasingly longer times and higher temperatures were required to achieve complete reaction with increasing Ho content. Completion of reaction, and therefore attainment of the state of equilibrium, was taken as reached when no further change in the phase assemblage(s) occurred, either on prolonged heating or by raising the temperature by 25–50 °C for an additional heating period. Thus, for compositions near the solid solution limit, determined to be $x = 0.175(25)$ at 1550 °C in the present study, reaction at 1550 °C for several days was necessary. This solid solution limit is slightly greater than reported in Ref. 7, $x = 0.14$, which may reflect both the higher reaction temperature and longer heating periods that were found necessary in this study to achieve equilibrium.

An additional complication found here and also noted in Ref. 7, was that the first product of reaction for high x compositions was the hexagonal polymorph of $BaTiO_3$ rather than the cubic polymorph. A careful study was therefore required to determine whether Ho stabilised thermodynamically the hexagonal polymorph of $BaTiO_3$, as presumed in Ref. 7, or whether it was a metastable phase that formed initially as a first product of synthesis, but subsequently transformed to the cubic phase on prolonged heating. In order to determine the thermodynamic status of the hexagonal polymorph it was necessary to establish the dependence of the cubic to hexagonal phase transformation temperature on Ho content; a series of isothermal heating experiments was therefore carried out on both stepwise heating and cooling, with the results summarised in Fig. 2. These results showed that for low x compositions, $0 \leq x \leq 0.05$, the cubic polymorph (which transformed to tetragonal during cooling to room temperature) was stabilised to increasingly higher temperatures with increasing x and that the transformation on heating, to give mixtures of (cubic + hexagonal) polymorphs, was fully reversible on stepwise cooling.

From these results, the phase diagram, Fig. 2, was constructed showing effective thermodynamic destabilisation of the hexagonal polymorph and therefore, stabilisation of the cubic polymorph, with increasing x. There was no evidence of significant doping of Ho under equilibrium conditions into the hexagonal structure, since the composition with the lowest Ho content, $x = 0.002$, gave a mixture of polymorphs at all temperatures studied from 1475 to 1550 °C. Therefore, the maximum Ho content that can be dissolved under equilibrium conditions into the hexagonal structure is $x < 0.002$ at $T \leq 1550$ °C.

Although the phase diagram shows that the hexagonal polymorph is increasingly unstable with increasing Ho content, nevertheless, as reported in Ref. 7, it does form in compositions with high Ho content. We therefore carried out a study of the effect of prolonged heating times on the products of reaction and found that with, for example, $x = 0.15$, the hexagonal polymorph formed initially but subsequently transformed to the cubic polymorph with prolonged heating. By adjusting the heat treatment conditions, it was possible to synthesise samples of single-phase hexagonal polymorph, e.g. for composition $x = 0.15$ heated at 1550 °C for 12 h. The conversion of this hexagonal polymorph to cubic with prolonged heating indicated that the hexagonal polymorph formed as a first product of reaction but was a metastable phase that transformed to the thermodynamically stable cubic polymorph on further heating.

In order to assess whether the composition(s) of the hexagonal and cubic polymorphs changed as a function of heat treatment, the lattice parameter of the cubic polymorph for composition $x = 0.15$ was measured as a function of hexagonal/cubic phase content, with the results shown in Fig. 3. There was no detectable systematic change in lattice parameter with phase content and the magnitude of a is the same as that for $x = 0.15$ demonstrated in a plot of lattice parameter vs. composition for the complete range of solid solutions, Fig. 4. The hexagonal to cubic transformation is, therefore, a very slow polymorphic change and does not involve any compositional change of the phases involved.

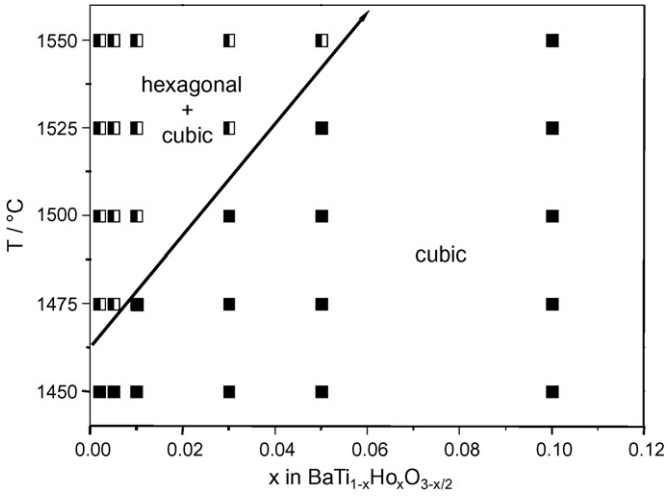

Fig. 2. High-temperature phase diagram showing cubic–hexagonal phase transformation.

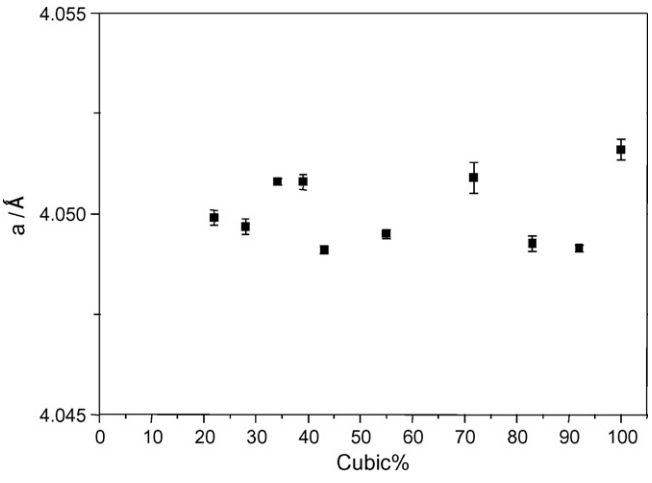

Fig. 3. Lattice parameter of the cubic solid solution in (cubic + hexagonal) two-phase mixtures during the hexagonal–cubic transformation.

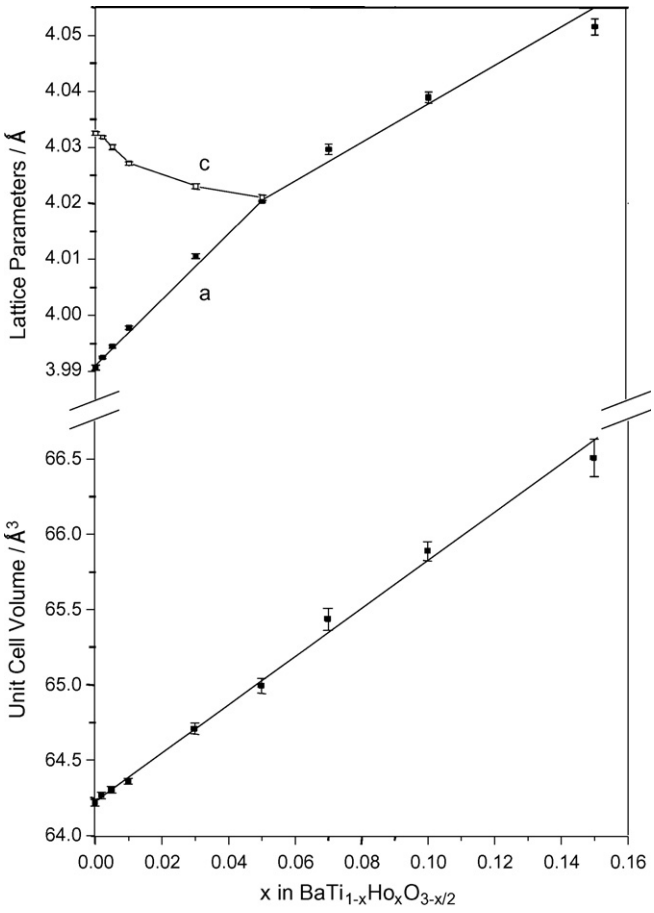

Fig. 4. Lattice parameters and cell volume as a function of composition.

The lattice parameter results in Fig. 4 confirm that, with increasing Ho content, the room temperature tetragonal polymorph gradually transforms to cubic and there is an overall increase in unit cell volume with increasing x, as expected from substitution of larger Ho onto the Ti site. The tetragonal–cubic transition is estimated to occur at the composition $x = 0.05(1)$ at room temperature.

The solid solution area for Ho-doped $BaTiO_3$, reported in Refs. 7,8 and shown in Fig. 1(b), shows very little evidence for significant solid solution formation according to mechanisms 3–5 for samples fired in air at 1400–1500 °C. This conclusion is confirmed from results obtained here on compositions $y = 0.04$ and $z = 0.02$, mechanisms 3 and 4, which showed phase mixtures after firing at 1450 °C. The rest of this paper focuses on the oxygen vacancy join, mechanism 1.

3.2. Electrical properties of $BaTi_{1-x}Ho_xO_{3-x/2}$

The electrical properties of ceramics fired under different conditions were measured using impedance spectroscopy and from data analysis, information was obtained on the electrical homogeneity of samples, together with values for the bulk and grain boundary conductivities and bulk permittivity as a function of temperature. In addition, fixed frequency values of permittivity were obtained by a rapid scan of electrical properties as a function of temperature and these values compared with those obtained by impedance spectroscopy analysis at a smaller number of fixed temperatures. For some samples, especially those with low x, subjected to rapid cool after firing at high temperatures, evidence of semiconductivity was seen, indicating that those samples had an additional doping mechanism, probably associated with oxygen loss. Further work on this effect is underway and will be reported subsequently. For the results presented here, samples were allowed to cool naturally in air on removing from the furnace or cooled inside the furnace at a slower rate and all samples studied were reasonably insulating.

A typical set of impedance data, for composition $x = 0.03$ fired at 1450 °C in air, is shown in Fig. 5. The impedance complex plane plot, (a), shows two arcs; for the same dataset, the Z"/M" spectroscopic plot, (b), shows two peaks in the Z" plot, corresponding to the two arcs shown in (a), whereas the M" plot shows a single peak corresponding to the higher frequency Z" peak. Since M" plots generally feature the bulk response of a sample which has the lowest capacitance, the high frequency peak is attributed to the sample bulk and the lower frequency Z" peak to an interfacial or grain boundary effect which has much larger capacitance and therefore is not readily apparent in the M" plot. Spectroscopic plots of capacitance, C', for this and a selection of other temperatures, are shown in (c). These show a constant high frequency capacitance value representing the sample bulk, which may be converted into bulk permittivity using, $\varepsilon' = C/C_0$, where C_0 is the vacuum capacitance of the measuring cell. The higher temperature data in (c) show an increase in C' at lower frequencies associated with the contribution of the interfacial or grain boundary capacitance.

In order to extract bulk permittivity values, it is clearly essential that the measuring frequency corresponds to the frequency-independent high frequency plateau region shown in (c). Fixed frequency data, at a frequency of 10^5 Hz, do correspond to this frequency-independent plateau over a wide temperature range and are shown in Fig. 6 as a function of temperature for $BaTiO_3$ and four compositions with different Ho content. Data for $BaTiO_3$ show the characteristic permittivity maxima corresponding, on cooling, to the cubic–tetragonal (132 °C), tetragonal–orthorhombic (28 °C) and orthorhombic–rhombohedral (−105 °C) transitions. With increasing Ho content, the cubic–tetragonal transition moves to lower temperature, that for the tetragonal–orthorhombic transition is essentially unchanged and that for the orthorhombic–rhombohedral transition appears to move to higher temperature. The net effect is that the three transitions coalesce, "pinching effect", to give a single broad peak for $x > \simeq 0.07$, as summarised in Fig. 7.

The permittivity data for low x compositions represent bulk permittivity values since, at 10^5 Hz, they are essentially independent of frequency, Fig. 5(c). For higher Ho contents, however, frequency-dependent relaxor behaviour is observed, as shown in Fig. 8, for $x = 0.07$. In this case, the permittivity is essentially independent of frequency above T_c, but shows a strong frequency-dependence below T_c. This effect is a bulk effect, distinguishable from the onset of interfacial or grain boundary capacitance that is generally observed in lower frequency

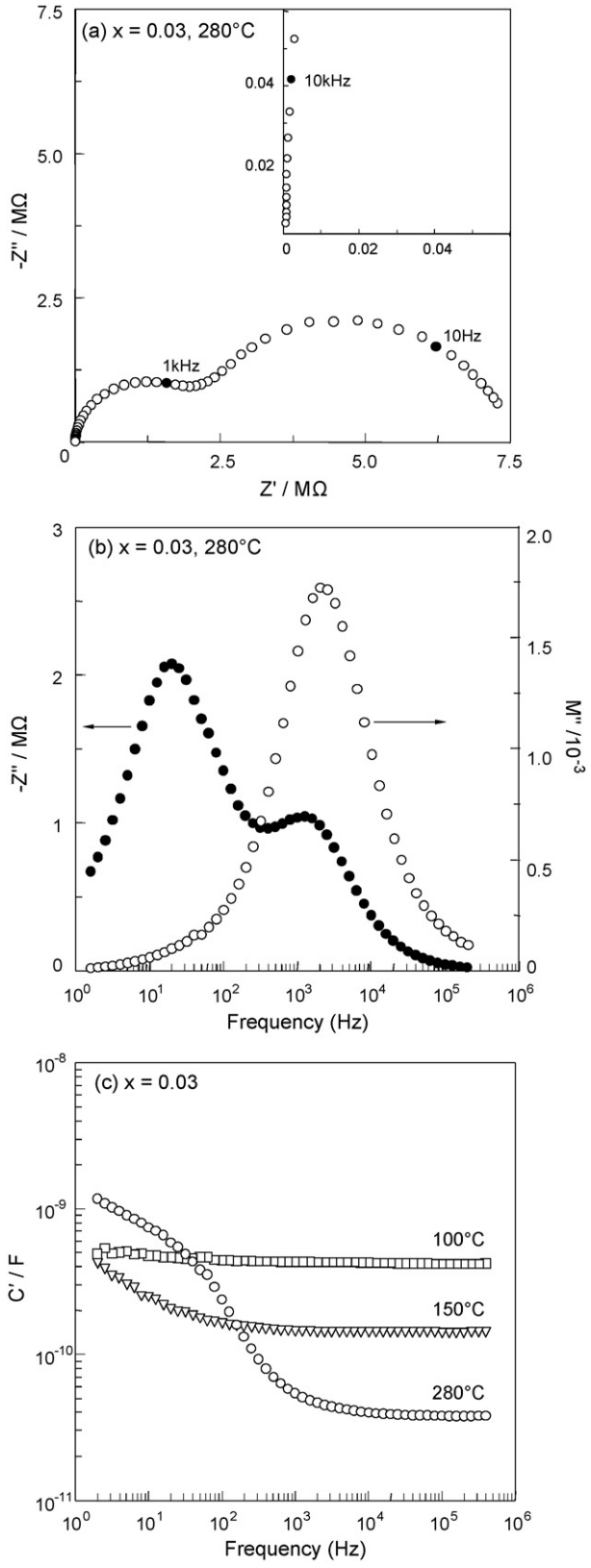

Fig. 5. Impedance data for one composition, $x = 0.03$ presented as (a) complex plane plot, (b) M''/Z'' spectroscopic plot and (c) C' spectroscopic plot. The sample was sintered in air at 1450 °C for 6 h; density ~90%.

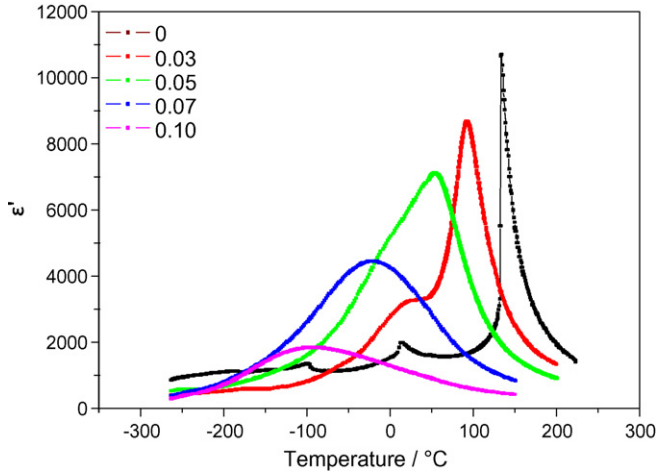

Fig. 6. Fixed frequency permittivity data as a function of temperature for $BaTiO_3$ and for Ho-containing compositions which were sintered in air at 1450 °C for 6 h.

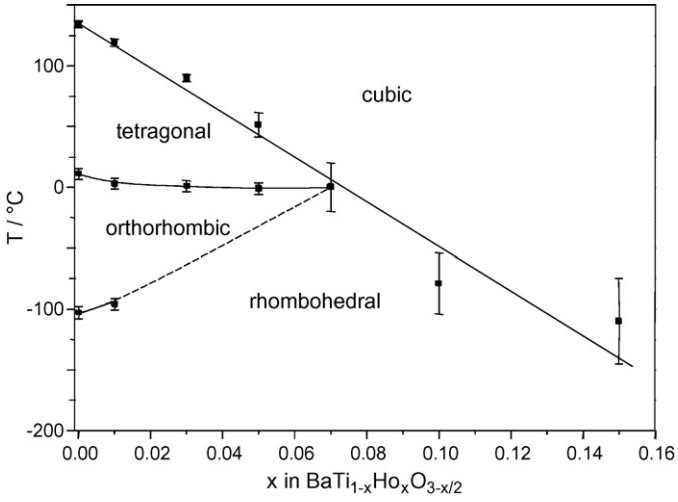

Fig. 7. Variation of phase transition temperatures with Ho-content.

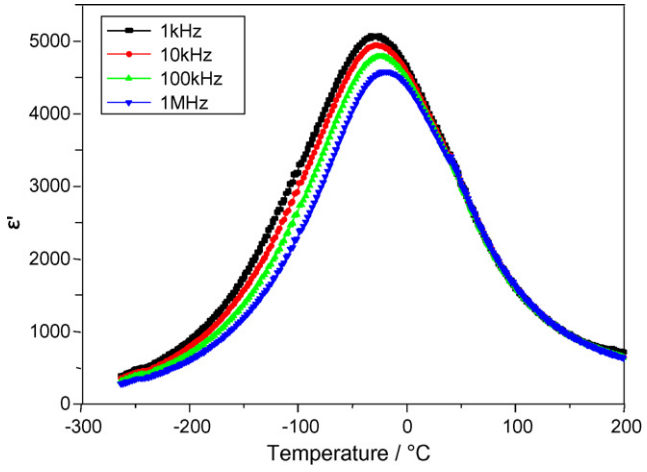

Fig. 8. Permittivity data for composition $x = 0.07$ showing relaxor behaviour.

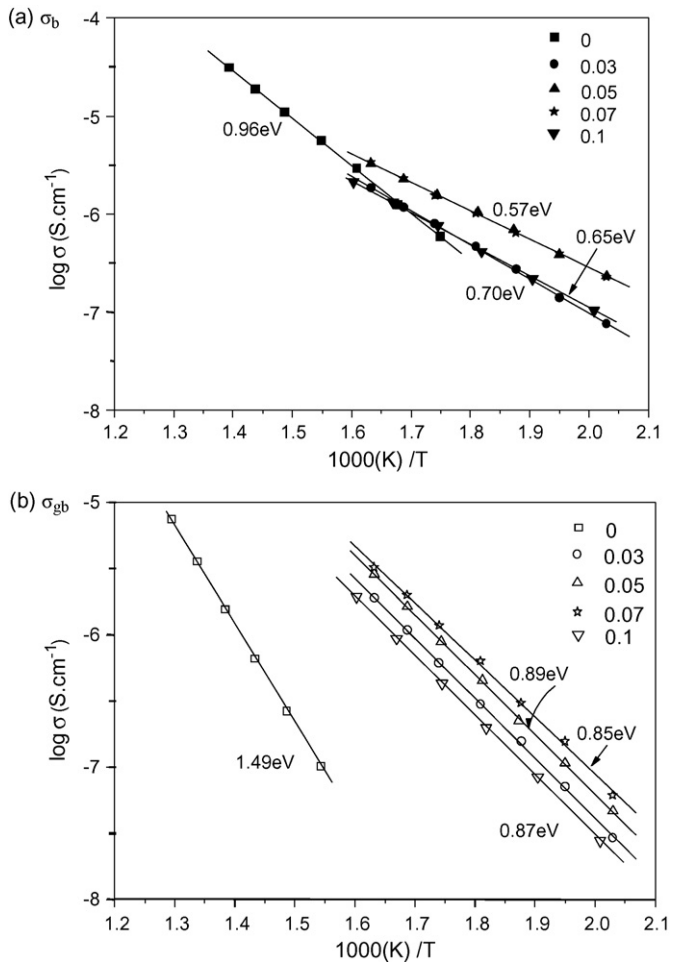

Fig. 9. Conductivity Arrhenius plots for bulk and grain boundary components. (a) σ_b and (b) σ_{gb}.

impedance data, Fig. 5(c). Further work to model this frequency dependence, using equivalent circuits, is in progress.

Conductivity data were extracted from impedance complex plane plots, as shown in Fig. 5(a) and are shown in Arrhenius format in Fig. 9. Bulk conductivities have activation energies in the range 0.6–0.7 eV and show little variation with Ho content. The materials are reasonably insulating with conductivity, e.g. $\sim 1 \times 10^{-6}\,\Omega^{-1}\,cm^{-1}$ at 300 °C. The interfacial or grain boundary conductivities are much lower, (b), and for all doped compositions have activation energies in the range of 0.85–0.90 eV, with little obvious dependence on composition. The grain boundary conductivity of undoped $BaTiO_3$ is much lower with higher activation energy, 1.49 eV, which probably represents a fully oxidised condition for the grain boundaries. For several reasons, we attribute the data shown in Fig. 9(b), which were extracted from the low frequency arc in Z^* plots, Fig. 5(a), to a grain boundary effect. For instance, the effect is not removed on polishing pellet surfaces and is not, therefore, a surface layer effect. Also, the Z^* data are not changed by application of a small *dc* bias and therefore it is not associated with a space charge effect such as a Schottky barrier at the electrode–pellet interface.

Hysteresis loop data for four compositions are shown in Fig. 10. Clear hysteresis loops are observed for $x = 0.01$, 0.03, 0.05, but with reductions in saturation polarisation, P_s, remanent polarisation, P_r and coercive field, E_c, with increasing x, consistent with a gradual loss in order within the ferroelectric domains and reduction in tetragonality of the overall crystal structure. Composition $x = 0.07$ shows a very thin hysteresis loop, (d), and for higher x values (not shown) the loop is entirely absent.

4. Discussion

An extensive range of Ho-doped $BaTiO_3$ solid solutions forms in which Ho substitutes for Ti with creation of oxygen vacancies as the charge compensation mechanism. The solid solution limit is $x = 0.175(25)$ at 1550 °C, which is slightly greater than $x = 0.14$ reported earlier,[7] but those data were for a lower temperature, 1400 °C; in addition, it was found here that with increasing Ho content, samples required heating for longer times and at higher temperatures in order to achieve complete reaction.

With increasing Ho content, the cubic–tetragonal ferroelectric phase transition temperature, T_c, moves to lower temperatures and this transition merges with the two lower temperature transitions, tetragonal–orthorhombic and orthorhombic–rhombohedral, such that a pinching effect occurs at $x \sim 0.07$. The variation of T_c with composition is ~20 °C/at.%Ho, which is comparable to that for substitution of La (24 °C)[5] and Ce (21 °C). Crystallographic studies to confirm the defect structure of the solid solutions have not been carried out, but from the single-phase nature of the samples and their locus in the $BaO–TiO_2–Ho_2O_3$ ternary composition diagram, it is highly likely that Ho substitutes directly for Ti on the octahedral sites in the perovskite structure. As the phase diagram studies[7] show, Ho is also able to substitute onto the Ba sites, but the present study focuses on limiting compositions which have Ho substituting exclusively for Ti.

The high-temperature hexagonal polymorph of $BaTiO_3$ is destabilised by substitution of Ho for Ti, as shown by an increase in the cubic–hexagonal phase transition temperature, with increasing x. This behaviour is the opposite of that seen with smaller dopant ions such as Mn, Fe[4], in which the dopant acts to stabilise the hexagonal form to lower temperatures.

In spite of this destabilisation of the hexagonal polymorph, Ho-rich compositions crystallised, as the first product of reaction, a solid solution of the hexagonal $BaTiO_3$ polymorph. This polymorph is kinetically stable only since, with prolonged heating at, e.g. 1550 °C, it gradually transformed to the cubic polymorph. It is therefore thermodynamically metastable, but forms as the kinetically stable first product of reaction. Its formation may be regarded as an example of Ostwald's rule of successive reactions in which a reaction pathway may proceed through a sequence of stages involving phases that are metastable under these reaction conditions before eventually yielding the thermodynamically stable product(s). This sequence of reactions may be rationalised in terms of free energy changes in which each successive phase assemblage has lower free energy than the preceding one. Possibly, the key driving force for the

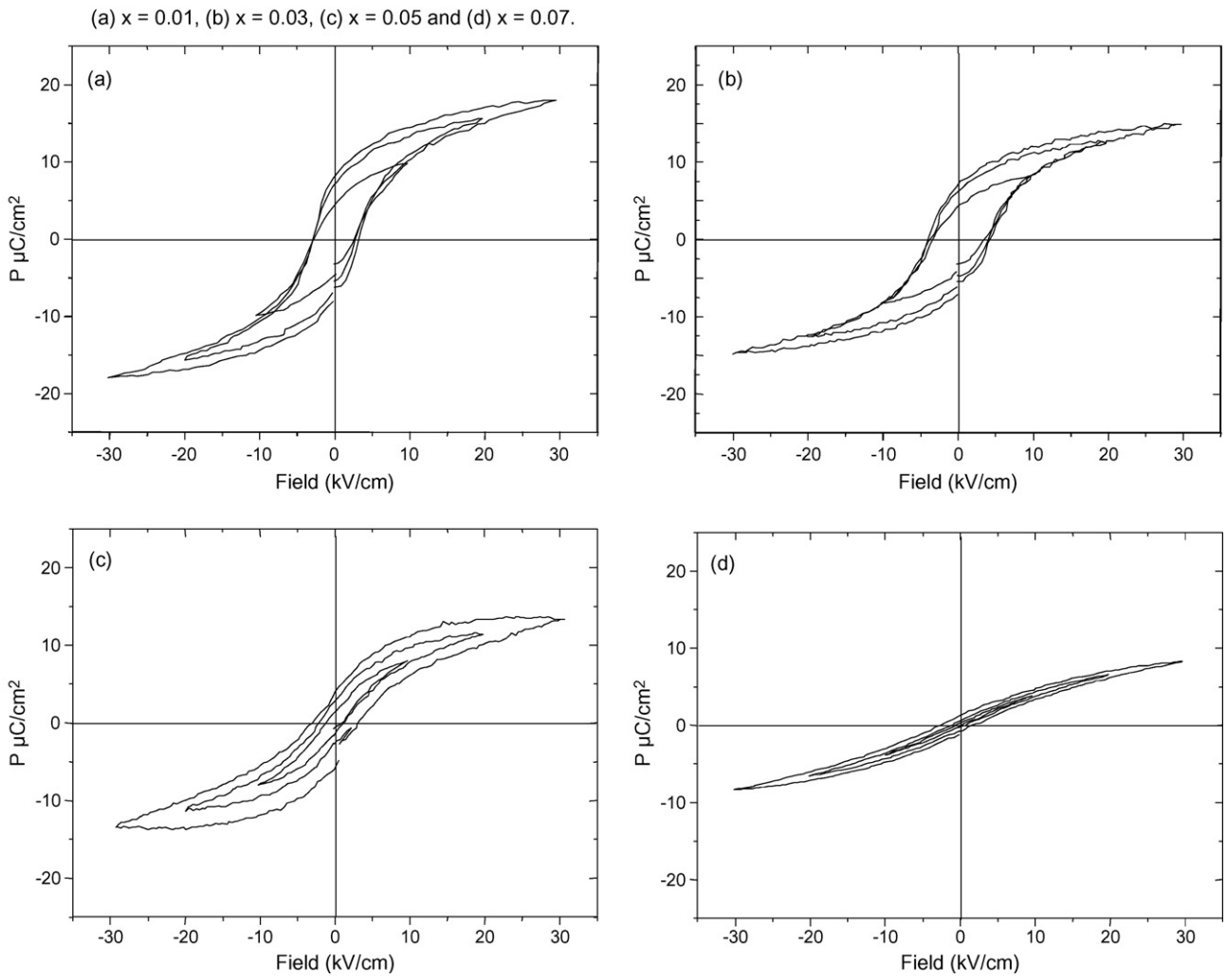

Fig. 10. Ferroelectric hysteresis loop data at room temperature for four compositions (a) $x = 0.01$, (b) $x = 0.03$, (c) $x = 0.05$, and (d) $x = 0.07$.

occurrence of intermediate stages is gradual reduction in entropy of the phase assemblages, commencing with the high entropy, disordered nature of the starting materials and terminating with the low entropy of the final crystalline product.

The electrical properties of ceramics of Ho-doped $BaTiO_3$ fired in air at 1400–1500 °C and cooled slowly were reasonably insulating, with evidence for both bulk and grain boundary components. Conductivity data for Ho-doped compositions were generally independent of x, but conductivity values, especially for the grain boundaries, were higher than those for undoped $BaTiO_3$. Although the conductivity data showed little composition dependence, permittivities were very composition-dependent and showed a reduction in both T_c and the magnitude of the permittivity at T_c with increasing x. For $x < 0.07$ sharp permittivity maxima were observed; at composition $x \simeq 0.07$, at which the three low temperature phase transitions in $BaTiO_3$ merged into a single transition, the permittivity profile became much broader and exhibited clear frequency-dependent relaxor behaviour. A similar transition from first order ferroelectric to relaxor ferroelectric has been observed in other doped $BaTiO_3$ materials; in each case, the change in ferroelectric behaviour coincides approximately with the pinching effect seen in the crystallographic phase transitions.

Acknowledgement

We thank EPSRC for financial support.

References

1. Kishi, H., Mizuno, Y. and Chazono, H., Base-metal electrode-multilayer ceramic capacitors: past, present and future perspectives. *Jpn. J. Appl. Phys.*, 2003, **42**(1), 1–15.
2. Huybrechts, B., Ishizaki, K. and Takata, M., Review – the positive temperature coefficient of resistivity in barium titanate. *J. Mater. Sci.*, 1995, **30**, 2463–2474.
3. Jo, S. K., Han, Y. H. and Choi, K. H., Effects of oxygen partial pressure control on the microstructure and PTCR properties of Ho-doped $BaTiO_3$. *J. Mater. Sci.*, 2007, **42**, 6696–6700.
4. Prades, M., Masó, N., Beltrán, H., Cordoncillo, E. and West, A. R., Polymorphism of $BaTiO_3$ acceptor doped with Mn^{3+}, Fe^{3+} and Ti^{3+}. *J. Am. Ceram. Soc.*, 2008, **91**, 2364–2366.
5. Morrison, F. D., Sinclair, D. C., Skakle, J. M. S. and West, A. R., Novel doping mechanism for very-high-permittivity barium titanate ceramics. *J. Am. Ceram. Soc.*, 1998, **81**, 1957–1960.

6. Morrison, F. D., Sinclair, D. C. and West, A. R., Characterization of lanthanum-doped barium titanate ceramics using impedance spectroscopy. *J. Am. Ceram. Soc.*, 2001, **84**(3), 531–538.
7. Makovec, D., Samardzija, Z. and Drofenik, M., Solid solubility of holmium, yttrium, and dysprosium in $BaTiO_3$. *J. Am. Ceram. Soc.*, 2004, **87**(7), 1324–1329.
8. Makovec, D., Samardzija, Z. and Drofenik, M., The solid solubility of holmium in $BaTiO_3$ under reducing conditions. *J. Am. Ceram. Soc.*, 2006, **89**(10), 3281–3284.
9. Chan, N. H., Sharma, R. K. and Smyth, D. M., Non-stoichiometry in acceptor-doped $BaTiO_3$. *J. Am. Ceram. Soc.*, 1982, **65**(3), 167–170.